Theor Chem Acc (2004) 112: 113–123
DOI 10.1007/s00214-004-0594-z

Theoretical
Chemistry Accounts

Regular article

Reduced-size representations of high-quality atomic densities. The hybrid Gaussian–exponential case

E. Francisco, L. Pueyo, A. Martín Pendás

Departamento de Química Física y Analítica, Facultad de Química, Universidad de Oviedo, E33006-Oviedo, Spain

Received: 7 March 2003 / Accepted: 18 June 2003 / Published online: 6 March 2004

Abstract. High-quality atomic electron densities are often approximated by limited-size expansions able to reproduce particular features of a reference function. Recent examples are the exponential sets of Koga [(2000)Theor. Chim. Acta 95: 113] and the Gaussian core densities of Cioslowski et al. [(1997) J. Chem. Phys. 106: 3607]. Since atomic densities have a rich structure and should obey theoretical conditions, the approximation procedure must be flexible enough to secure useful results. Here we present an extension of the algorithm used by Koga that gives uniformly accurate densities even for hybrid Gaussian–exponential sets. We report approximate densities of this type for the ground state of neutral atoms He–Xe that exactly copy the reference density and its first and second derivatives at $r = 0$, describe accurately the finer details of the density convex structure, reproduce its most significant moments, and give a faithful description of the Z dependence of density functionals like $\langle \rho^{-1/3} \rangle$ or the Shannon entropy.

Keywords: Atomic electron density – Hartree–Fock – Neutral atoms

1 Introduction

The spherically averaged ground-state electron density $\rho(r)$ of neutral atoms has always been a very important concept in atomic research. It is lately receiving much attention, for it has found important applications in a number of fields that demand accurate and workable atomic electron densities, either complete or corelike.

Quantum mechanical simulations of large systems almost necessarily invoke simplifications such as the use of pseudopotentials or model potentials to account for the chemically inactive core electrons. This results in vast computer time savings at the expense of producing pseudodensities. However, significant observables such as hyperfine interactions, electric field gradients at the nuclei, or X-ray structure factors depend on the complete density. Moreover, the most successful theories of the chemical bond—like the theory of atoms in molecules [1] or the studies on the electron localization function [2, 3, 4]—are based on the topological behavior of scalar fields dependent on the full electron density. The difficulties of the pseudopotential approximation in these cases lead to the reconstruction of complete densities from pseudodensities [5, 6, 7, 8], a task that requires reliable descriptions of the atomic cores.

On the other hand, chemical studies of X-ray-derived charge densities, now routine [9], rely on the a priori knowledge of a model crystalline electron density that is further allowed to relax in a number of ways (i.e. multipole deformation, radial breathing, etc.). The independent atom model (IAM), in which the crystal (molecule) is approximated as a procrystal (promolecule) defined as the superposition of spherical densities of the isolated atoms, is invariably used to construct the initial density model. The quality of the IAM cores used determines in an essential way that of the final densities. For example, no reliable density derivatives near the nuclei may be obtained with the very small analytical representations of the IAM densities used just some years ago.

Furthermore, the Hirshfeld partitioning of the electron density [10], together with the IAM, have also been used by Spackman and coworkers [11, 12, 13] to show that the crystalline density can be divided into molecular fractions that permit univocal definitions of molecular surfaces and volumes, as well as a straightforward calculation of average quantities by direct integration over the weighted density. The computational advantages of these Hirshfeld surfaces, which are the isosurfaces of the molecular weight function $w(\mathbf{r}) = \rho_{\text{promolecule}}(\mathbf{r})/\rho_{\text{procrystal}}(\mathbf{r})$ corresponding to $w = 0.5$, heavily rest upon the availability of suitable analytical expressions for the atomic densities. In a different but related context, Martín Pendás et al. [14] discuss the advantages of the

Correspondence to: E. Francisco
e-mail: evelio@carbono.quimica.uniovi.es

IAM in the topological analysis of the electron density of ionic crystals.

For years, the nonrelativistic Hartree–Fock–Roothaan (HFR) atomic functions of Clementi and Roetti [15] and McLean and McLean [16] were nearly universal references in this field. Later on, more accurate atomic densities were reported by Bunge et al. [17] and Koga and coworkers [18, 19, 20, 21]. These high-quality Slater-type densities, however, contain a number of $r^{n_i}\mathrm{e}^{-\zeta_i r}$ terms simply too large to be appropriate for research work on complex systems. Fortunately, Koga [22] has recently shown that a much smaller representation of the atomic density can be found by careful fitting of a suitable analytical expression to the high-quality densities. Such analytical approximations can be designed to fulfil specific requirements not necessarily satisfied if the standard HFR procedure over the corresponding basis set is performed. With a similar strategy, Cioslowski et al. [23] obtained accurate analytical representations of the relativistic core–electron densities of elements 3–118 which are made of 50 s-type Gaussian terms. These core–electron densities are useful tools for many types of calculations and analyses, from the quantum-mechanical theory of atoms in molecules [1] to the experimental determination of molecular densities from X-ray diffraction measurements. However, the Gaussian densities do not satisfy the Kato nucleus–electron cusp condition [24], one of the few structural properties of the atomic electron density known in analytical form. This and other relations of this sort, such as the differential inequality for $\rho(r)^{1/2}$ of the Hoffmann–Ostenhof expression [25] or the large–distance $r^{2\beta}\mathrm{e}^{-2\alpha r}$ asymptotic form [with $\beta = (Z - N + 1)/\alpha - 1$, $\alpha = \sqrt{2\epsilon}$, and ϵ being the ionization potential of the N-electron atom of atomic number Z] [26, 27] might be very significant attributes of the approximate density, depending upon the target established in its design. For instance, the convex structure of the electron density may become a very relevant target in the research of nonnuclear maxima of the molecular or crystal densities [28].

These arguments call for powerful and flexible approximation procedures, able to accommodate in a systematic manner the various theoretical requirements imposed upon a reduced-size atomic density. We present in this work results of our investigation on the Lagrangian algorithm used by Koga [22] in reproducing high-quality numerical HFR atomic densities in terms of exponential sets with fewer than 30 primitive functions. We show here that this algorithm is easily formulated in a simple algebraic form that permits the immediate incorporation of new constraints with a minimum amount of work. We have found that inclusion of the constraint of an exact copy of the second derivative of the reference density at $r = 0$ improves significantly the conduct of the approximate density near the nucleus. The power of the algorithm is demonstrated by considering hybrid densities made of a reduced Gaussian set plus a single exponential function. Such peculiar forms display the appropriate behavior at very short and large distances and uniformly satisfy the known theoretical conditions operating on the electron atomic density. This mathematical result has been obtained for the large majority of ground–state densities of neutral atoms He–Xe. Moreover, we examine a collection of structural properties of densities of this form that were not considered in Ref. [22]. We believe that it is important to document the very good response of both the reference and the approximate densities to a wide set of very demanding tests, of relevance in a variety of theoretical and computational fields.

In the next section we describe the approximation procedure with a minimum of computational details. The more relevant results are presented and discussed in Sect.3. The last section collects our conclusions. Atomic units are used throughout.

2 The approximation procedure

Given a reference atomic electron density $\rho(r)$, we consider an analytical approximation to it of the form

$$F(r) = f_0(r) + \mathbf{f}^{\dagger}(r)\mathbf{C} \ , \tag{1}$$

where

$$f_0(r) = A\rho(0)\exp(-2Zr) \ , \tag{2}$$

where Z is the atomic number, $\mathbf{f}(r)$ is a p-dimensional column vector with elements

$$f_i(r) = \exp(-\zeta_i r^2) \ , \tag{3}$$

and the scalar A, the p components of the column vector $\mathbf{C}$, and the orbital exponents ζ_i, collected in the column vector $\mathbf{Z}$ are fitting parameters. For reference densities with $\rho(0) \neq 0$, $F(r)$ approaches the origin exponentially as $A\rho(0)(1 - 2Zr) + \mathbf{1}_p^{\dagger}\mathbf{C}$, for $r \ll 1$. $\mathbf{1}_p$ is the p-dimensional column vector having all components equal to unity. If $\rho(0) = 0$, $F(r)$ becomes a pure Gaussian density, approaching the origin as $(\mathbf{1}_p^{*} - \mathbf{Z}^{\dagger}r^2)\mathbf{C}$ for $r \ll 1$.

The $2p + 1$ free parameters in $F(r)$ are chosen to match $\rho(r)$ as closely as possible, particularly in the regions where it is large and in the range of r relevant to chemical bonding. To reach these goals we minimize the mean square deviation

$$\begin{aligned}\Delta(\mathbf{C},\mathbf{Z}) &= 4\pi\int_0^{\infty}\delta(r)^2 r^2 \mathrm{d}r \\ &= 4\pi\int_0^{\infty}[\rho(r) - F(r)]^2 r^2 \mathrm{d}r \\ &= 4\pi\int_0^{\infty}[\bar{\rho}(r) - \mathbf{f}^{\dagger}(r)\mathbf{C}]^2 r^2 \mathrm{d}r \ ,\end{aligned} \tag{4}$$

with $\bar{\rho}(r) = \rho(r) - f_0(r)$, under a series of constraint conditions incorporated by the method of Lagrange multipliers. Cioslowski et al. [23] weighted the deviation $\delta(r)$ in Eq. (4) with the inverse of the reference density as a compromise between the unweighted fitting, which gives worse results at places of small density, and the $\rho(r)^{-2}$ weight, that gives rise to difficulties when $\rho(r)$ is

large. We use the unweighted deviation to have good fitting near the nucleus, the exponential component favoring the copying at large distances.

Equation (4) can be written in matrix form:

$$\Delta(\mathbf{C},\mathbf{Z}) = \Delta_0 - 2\mathbf{G}^\dagger\mathbf{C} + \mathbf{C}^\dagger\mathbf{S}\mathbf{C} \ , \tag{5}$$

where

$$\Delta_0 = 4\pi \int_0^\infty \bar{\rho}^2(r) r^2 \mathrm{d}r \ , \tag{6}$$

$$\mathbf{G} = 4\pi \int_0^\infty \bar{\rho}(r)\mathbf{f}(r) r^2 \mathrm{d}r \tag{7}$$

is a p-dimensional column vector, and

$$\mathbf{S} = 4\pi \int_0^\infty \mathbf{f}(r)\mathbf{f}^\dagger(r) r^2 \mathrm{d}r \tag{8}$$

is the $p \times p$ metric matrix of the $F(r)$ Gaussian subset.

As constraint conditions we select the following. First, we want $F(r)$ and its first and second derivatives to exactly reproduce the corresponding reference values at the origin, i.e.

$$1.\ F(0) = \rho(0) \tag{9}$$

$$2.\ F'(0) = \rho'(0) \tag{10}$$

$$3.\ F''(0) = \rho''(0) \ . \tag{11}$$

Condition 1 implies

$$\mathbf{1}_p^\dagger\mathbf{C} = \rho(0)(1-A) \ . \tag{12}$$

Equations (9) and (10) show that $F(r)$ fulfils the cusp condition if $\rho(r)$ does. This is at variance with Koga's approach [22], that forces $F(r)$ to fulfil this condition in any case, even if the reference density does not. From Eq. (10), we find

$$A = -\frac{\rho'(0)}{2Z\rho(0)} \ , \tag{13}$$

showing that if $\rho(r)$ fulfils the cusp condition, $A = 1$ and, from Eq. (12), $\mathbf{1}_p^\dagger\mathbf{C} = 0$. Using Eqs. (12) and (13), we can write

$$\mathbf{1}_p^\dagger\mathbf{C} = F(0) + \frac{F'(0)}{2Z} = \rho(0) + \frac{\rho'(0)}{2Z} = g(0) \ . \tag{14}$$

Condition 3 restricts the $\zeta_i C_i$ products in say, the form

$$2\mathbf{Z}^\dagger\mathbf{C} = -\rho''(0) - 2Z\rho'(0) = h(0) \ . \tag{15}$$

This constraint is a further difference with the criteria adopted by Koga [22].

At this point, we recall that the choice $A = 1$ may produce numerical instabilities in the optimization process. The value given by Eq. (13), however, avoids such difficulties and makes the algorithm more general and independent of whether the reference density fulfils the cusp condition or not. Constraints 1, 2, and 3, expressed in the forms of Eqs. (14) and (15), incorporate this option for A.

Finally, we try to copy the structure of $\rho(r)$ in the range of chemical interest by forcing $F(r)$ to reproduce inner and outer $\langle r^k \rangle$ moments of $\rho(r)$, namely $k = -2, \ldots, +6$. These are demanding and significant restrictions since the density may be characterized by these moments. Thus, we have nine further condition equations,

$$4\pi \int_0^\infty [F(r) - \rho(r)] r^{k+2} \mathrm{d}r = 0 \ , \tag{16}$$

that can be written in the form

$$\mathbf{T}^\dagger\mathbf{C} - \mathbf{D} = 0, \quad (k = -2, \ldots, +6) \ . \tag{17}$$

In this equation, the p-dimensional column vectors

$$\mathbf{T}_k = 4\pi \int_0^\infty \mathbf{f}(r) r^{k+2} \mathrm{d}r, \quad k = -2, \ldots, 6 \ , \tag{18}$$

are collected in the $p \times 9$ $\mathbf{T}$ matrix, and the numbers

$$D_k = 4\pi \int_0^\infty [\rho(r) - f_0(r)] r^{k+2} \mathrm{d}r \tag{19}$$

in the nine-dimensional column vector $\mathbf{D}$. In this way, $\mathbf{T}^\dagger\mathbf{C} - \mathbf{D}$ is a nine-dimensional column vector.

The appropriate Lagrange function for the conditional minimization of $\Delta(\mathbf{C},\mathbf{Z})$ in Eq. (5) is

$$\begin{aligned}\Lambda(\mathbf{C},\mathbf{Z}) = \Delta_0 - 2\mathbf{G}^\dagger\mathbf{C} + \mathbf{C}^\dagger\mathbf{S}\mathbf{C} - \mathbf{L}^\dagger(\mathbf{T}^\dagger\mathbf{C} - \mathbf{D}) \\ - \mu[\mathbf{1}_p^\dagger\mathbf{C} - g(0)] - \nu[2\mathbf{Z}^\dagger\mathbf{C} - h(0)] \ ,\end{aligned} \tag{20}$$

where the nine λ_k multipliers associated with the $\langle r^k \rangle$ constraints (Eq. 16) are collected in the $\mathbf{L}$ column vector, and μ and ν are the multipliers associated with the constraints at the origin (Eqs. 9, 10, 11).

The conditions that make $\Lambda(\mathbf{C},\mathbf{Z})$ stationary are

$$\frac{\partial\Lambda}{\partial\mathbf{C}} = -2\mathbf{G} + 2\mathbf{S}\mathbf{C} - \mathbf{T}\mathbf{L} - \mu\mathbf{1}_p - 2\nu\mathbf{Z} = 0 \ , \tag{21}$$

$$\frac{\partial\Lambda}{\partial\mathbf{L}} = \mathbf{T}^\dagger\mathbf{C} - \mathbf{D} = 0 \ , \tag{22}$$

$$\frac{\partial\Lambda}{\partial\mu} = \mathbf{1}_p^\dagger\mathbf{C} - g(0) = 0 \ , \tag{23}$$

$$\frac{\partial\Lambda}{\partial\nu} = 2\mathbf{Z}^\dagger\mathbf{C} - h(0) = 0 \ , \tag{24}$$

or, in a more compact form

$$\begin{pmatrix} 2\mathbf{S} & -\mathbf{T} & -\mathbf{1}_p & -2\mathbf{Z} \\ \mathbf{T}^\dagger & \mathbf{0} & \mathbf{0} & \mathbf{0} \\ \mathbf{1}_p^\dagger & \mathbf{0} & \mathbf{0} & \mathbf{0} \\ 2\mathbf{Z}^\dagger & \mathbf{0} & \mathbf{0} & \mathbf{0} \end{pmatrix} \begin{pmatrix} \mathbf{C} \\ \mathbf{L} \\ \mu \\ \nu \end{pmatrix} = \begin{pmatrix} 2\mathbf{G} \\ \mathbf{D} \\ g(0) \\ h(0) \end{pmatrix} \ . \tag{25}$$

For a given $\mathbf{Z}$ vector, Eq. (25) is a linear system of $p + 11$ equations with $p + 11$ unknowns that gives the solutions $\mathbf{C}_{\mathrm{opt}}$, $\mathbf{L}_{\mathrm{opt}}$, μ_{opt}, and ν_{opt}. The Lagrange

function (Eq. 20) evaluated at this solution gives the optimum deviation

$$\Delta_{\text{opt}} = \Delta_0 - 2\mathbf{G}^{\dagger}\mathbf{C}_{\text{opt}} + \mathbf{C}_{\text{opt}}^{\dagger}\mathbf{S}\mathbf{C}_{\text{opt}} \ . \tag{26}$$

This scheme can easily be extended to make higher-order even derivatives $F^{2n}(0)$ equal to $\rho^{2n}(0)$. Odd derivatives cannot be considered because the identification $F^{2n+1}(0) = \rho^{2n+1}(0), (n = 1, 2, \ldots)$ does not contain free parameters. The general even-derivative condition, in the form of Eqs. (14) and (15), is

$$(-1)^n \frac{(2n)!}{n!}(\mathbf{Z}^{\mathbf{n}})^{\dagger}\mathbf{C} = \rho^{2n}(0) - (-2Z)^{2n} A\rho(0) \ , \tag{27}$$

where $(\mathbf{Z}^{\mathbf{n}})^{\dagger} = (\zeta_1^n, \ldots, \zeta_p^n)$. Each of these constraint equations introduces a new Lagrange multiplier, a new row, and a new column in the linear transformation (Eq. 25).

To conclude this section, we recall that the matrix elements of the **T** matrix are

$$T_{ik} = 2\pi\zeta_i^{-(k+3)/2}\Gamma\left(\frac{k+3}{2}\right) \ , \tag{28}$$

and those of the **S** matrix are

$$S_{ij} = \left(\pi/\zeta_{ij}\right)^{3/2}, \quad \zeta_{ij} = \zeta_i + \zeta_j \ . \tag{29}$$

To compute the **G** vector we have to specify the form of $\bar{\rho}(r)$, a function that can be obtained from numerical Hartree–Fock or multiconfigurational Dirac–Fock calculations. In this paper, we use the reference atomic density given by Koga et al. [21]. Since this is a Slater-type density, $\bar{\rho}(r)$ can always be written in the form

$$\bar{\rho}(r) = \sum_j b_j r^{m_j} \exp\left(-\sigma_j r\right) \ . \tag{30}$$

Then, the G_i element becomes

$$G_i = 4\pi \sum_j b_j \int_0^{\infty} r^{m_j+2} \mathrm{e}^{-\zeta_i r^2} \mathrm{e}^{-\sigma_j r} \mathrm{d}r \ . \tag{31}$$

The basic integral

$$I(\zeta, \sigma, s) = \int_0^{\infty} r^s \mathrm{e}^{-\zeta r^2} \mathrm{e}^{-\sigma r} \mathrm{d}r \tag{32}$$

can be computed analytically but its numerical evaluation avoids the instabilities that may appear for certain $[\zeta, \sigma]$ pairs. To perform this integration, we first transform r to $\bar{r} = \sqrt{\zeta} r$ and obtain

$$I(\zeta, \sigma, s) = \zeta^{-(s+1)/2} I(1, \sigma', s) \ , \tag{33}$$

where $\sigma' = \sigma\zeta^{-1/2}$. Then $\bar{r} \in [0, \infty)$ is mapped into $u \in [-1, +1]$ by the transformation

$$\bar{r}(u) = \bar{r}_{\text{m}}\left(\frac{1+u}{1-u}\right) \ , \tag{34}$$

where

$$\bar{r}_{\text{m}} = \frac{-\sigma' + \left(\sigma'^2 + 8s\right)^{\frac{1}{2}}}{4} \tag{35}$$

is the value of $\bar{r}$ for which the integrand of $I(1, \sigma', s)$ is a maximum. Then, Eq. (32) becomes

$$I(\zeta, \sigma, s) = 2r_{\text{m}}\zeta^{-(s+1)/2} \int_{-1}^{+1} F[r(u)]\mathrm{d}u \ , \tag{36}$$

where

$$F[r(u)] = \frac{r^s(u)}{(1-u)^2} \mathrm{e}^{-r^2(u)} \mathrm{e}^{-\sigma' r(u)} \mathrm{d}u \ . \tag{37}$$

The integral in Eq. (36) is finally computed with a relative error smaller than $\varepsilon = 10^{-12}$ using the numerical integration scheme of Pérez–Jordá and coworkers [29].

Finally, to avoid a prohibitive computational effort in optimizing the Gaussian exponents $\zeta_i \in \mathbf{Z}$, we follow the even-tempered recipe [22, 23]

$$\zeta_i = \alpha\beta^{i-1}, \quad (i = 1, \ldots, p) \ . \tag{38}$$

Optimum values of α and β were obtained by minimizing Δ_{opt} (Eq. 26) by means of a conjugate gradient method which does not compute derivatives [30].

3 Results and discussion

3.1 Control of the fitting

As a rule, the minimization of Δ_{opt} (Eq. 26) for the atom with atomic number Z used input values of α and β taken from the optimum values found for the atom with atomic number $Z - 1$. When this strategy was used and the run ended successfully giving $\Delta_{\text{opt}} \sim 10^{-10}$ or smaller the optimization was accepted. For many atoms, this procedure works very well and the optimization ends very quickly. For some others, however, we had to stop the minimization and start it again with fresh input values of α and β. We found no systematic way of altering the input values of these parameters when the general strategy fails to give an acceptably small value of Δ_{opt}. In these problematic atoms, we generally found several local minima and could not establish for sure if the lowest minimum had or had not been located. Moreover, we observed that optimum deviations differing by an order of magnitude or more can be reached with sets of (α, β) pairs very close to each other. Our best deviation is smaller than 10^{-7} in all the cases, except for Al, Si, P, S, and Cl, where we were unable to find deviations smaller than this number with $p \leq 25$. For the Cu–Se set, we needed 25 Gaussian primitives to obtain acceptable deviations; all other cases required just 20 terms. To analyse further the reasons behind the poor behaviour of the fitting procedure in the problematic cases we repeated it using as a reference the Clementi and Roetti densities [15]. In the 11 cases (Al, Si, P, S, Cl, Cu–Se) except Zn, we obtained Δ_{opt} values smaller than 10^{-12}. This fact clearly evidences that the quality of the fitting depends to a great extent on the reference density and less on the atomic number, configuration, or electronic state of the atom.

The variation of α and β with the atomic number Z is better appreciated in Fig 1. The smallest orbital

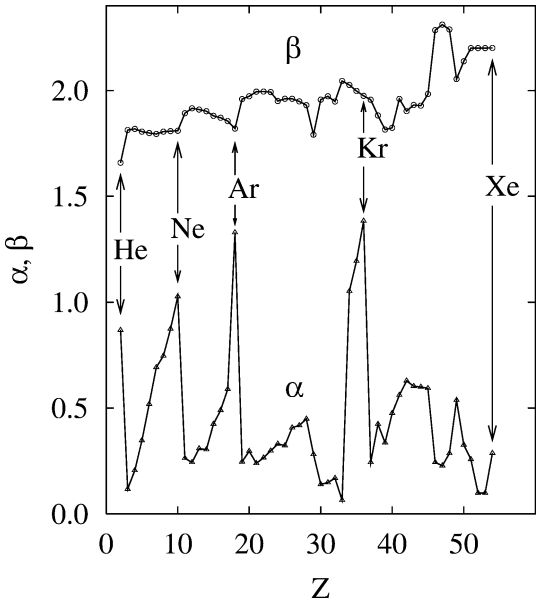

Fig. 1. Optimum values of α and β, Eq. (38), for He–Xe. α has been scaled by a factor 10.0

exponent $\zeta_{\min} = \alpha$ shows a clear shell structure with rare-gas atoms at the peaks and alkaline atoms at the bottom line. The best β, however, is roughly constant along each period, with the exception of the last one (Rb–Xe), where it shows a rather erratic trend.

The values of $\rho(0)$, the scalar A in Eq. (13), α and β, Eq. (38), the $r_{\max}$ coordinate giving the maximum $|\delta(r)|$ in Eq. (4), and the relative error $\epsilon = 100\times |\delta(r_{\max})|/\rho(r_{\max})$ are collected in Table 1. The values of A show that the cusp condition is neither fulfilled by the reference densities nor by the approximate ones. We see that $A < 1$ for He, B–O, and Cl, and $A > 1$ for all other atoms. We comment on this difference in the next subsection. The sixth column shows that the largest deviation of the approximate density appears at very internal regions: $r_{\max}$ is smaller than 0.07 bohr for all cases. The relative error ϵ is smaller than 10^{-1} for all atoms but Y and Cd, where it is abnormally high; it is smaller than 10^{-2} for 33 out of the 53 atoms. As a typical example, some detailed results for the Fe atom are presented in Table 2.

3.2 Nonnegativity, convexity, and shell structure of the approximate density

We have checked the nonnegativity of $F(r)$. Mo and In showed in the initial fittings some negative values of $F(r)$, probably owing to the restrictions of the innermost $\langle r^k \rangle$ moments. A calculation for these two atoms with $k_{\min} = 0$ instead of $k_{\min} = -2$ gives nonnegative $F(r)$ for any r, with relative errors for $\langle r^{-2} \rangle$ ($\langle r^{-1} \rangle$) of 2.9×10^{-4} (9.6×10^{-4}) and 5.2×10^{-4} (1.65×10^{-3}) for Mo and In, respectively. No other atom gives $F(r) < 0$ in the range $0 \le r \le 9.0$ bohr. For $r > 9.0$ bohr, any negative density is always smaller than 10^{-7} in absolute value. It is also worth mentioning that removal of the restrictions of the innermost moments ($k = -2$ and $k = -1$) gives $F(r)$ functions that reproduce very well the reference values of these two integrals. However, removal of the constraints associated with $k = 1 - 6$ gives $F(r)$ functions with unacceptable relative errors for the corresponding moments, at least in some cases. This numerical result shows the importance of the $\langle r^k \rangle$ ($k = 1 - 6$) constraints in determining the approximate density in regions of chemical interest.

A global view of the quality of the fitting can be seen in Fig. 2, where we compare $F(r)$ and its first and second derivatives with the corresponding reference functions for sulfur ($0.001 < r < 9.3$ bohr). We find similar results for all atoms. The good performance of $F(r)$, $F'(r)$, and $F''(r)$ in this range of r is apparent. The behaviour of the derivatives is particularly satisfactory because it is not enforced by the algorithm. The inset in this figure shows that the approximate density reproduces in detail the small nonconvexity region of the reference density for this atom.

A detailed examination of the $F(r)$ density can be done in terms of the radial functions

$$A(r) = -\frac{\rho'(r)}{2Z\rho(r)} \qquad B(r) = -\frac{\rho''(r)}{2Z\rho'(r)} \quad . \tag{39}$$

To see these functions for the two atoms with large relative errors (last column of Table 1), namely, Y and Cd, we plot $A(r)$ for Cd ($0.0001 \le r \le 8.4$ bohr) in Fig. 3 and $B(r)$ for Y ($0.0001 \le r \le 10.3$ bohr) in Fig. 4. The complete oscillatory structure of these functions is reproduced by the approximate densities. For larger distances, the fitting progressively deteriorates but the density is already smaller than 10^{-8}.

The $A(r)$ function becomes the scalar A, Eq. (13), at the nucleus. Table 1 shows that the reference and the approximate densities give values for A very close to but different from unity. Koga's density has, for most atoms up to Xe, a small region close to the nucleus where $A(r) > 1$, but a group of six elements (He, B, C, N, O, and Cl) have $A(r) < 1$ for $0 \le r \le \infty$. Gálvez and Porras [31, 32] conjectured that the function $g(r) = \rho(r) + \rho'(r)/2Z = \rho(r)[1 - A(r)]$ is positive everywhere. We observe that in Koga's representation $g(r)$ has a small region near the nucleus where it is negative for atoms Li–Xe, with the exceptions of B, C, N, O, and Cl.

We also analysed whether $F(r)$ reproduces or not the convex structure of $\rho(r)$. This property was investigated by Angulo and coworkers [33, 34, 35, 36, 37, 38] for $Z \le 54$ using the ground–state HFR solutions of Clementi and Roetti [15]. They found that neutral atoms with $Z = 1, 2, 7 - 15$, and 33–44 have a convex density. Esquivel et al. [26] showed that strict pseudoconvexity $[(r_1 - r_2)\rho'(r) \ge 0$ implies $\rho(r_1) \ge \rho(r_2)]$ is the general structural property of the electron density of the neutral atoms. They extended the numerical analysis to all atoms with $Z \le 92$ using the bare Coulomb field (BCF) approximation, the Hartree–Fock level, and highly correlated wave functions, and showed that the nonconvexity of $\rho(r)$ is a periodical property whose origin can be ascribed to the BCF of the atom [27]. Here we use their type of plots [27] to show the Z dependence of the

Table 1. Summary of results for atoms He–Xe. The dimension of the **f**(r) vector in Eq. (2) is $p = 20$ in all cases except in the Cu–Se group, where $p = 25$. r_{max} is the coordinate of the highest deviation in Eq. (4). ϵ is the relative error of the approximate density

Atom	$\rho(0)$	A, Eq. (13)	α, Eq. (38)	β, Eq. (38)	r_{max}	ϵ (%)
He	0.3595875124×10^{1}	0.999913	0.0868033775	1.6587545566	0.048921	0.000
Li	0.1381509394×10^{2}	1.000142	0.0116723101	1.8132088461	0.065830	0.002
Be	0.3538901529×10^{2}	1.000269	0.0205262078	1.8183983077	0.046956	0.001
B	0.7192019892×10^{2}	0.999875	0.0346918575	1.8058375895	0.017700	0.001
C	$0.12741568785\times10^{3}$	0.999935	0.0518650363	1.7988504058	0.014750	0.001
N	0.2059662847×10^{3}	0.999920	0.0692063825	1.7947898357	0.012643	0.001
O	0.3116597037×10^{3}	0.999967	0.0746499286	1.8056476734	0.011632	0.001
F	$0.44832243011\times10^{3}$	1.000000	0.0873899901	1.8080047184	0.010871	0.001
Ne	0.6199243910×10^{3}	1.000025	0.1026647887	1.8095035595	0.009784	0.001
Na	0.8337671053×10^{3}	1.000075	0.0263200911	1.8925419771	0.029650	0.003
Mg	0.1093726466×10^{4}	1.000056	0.0243418861	1.9157128693	0.012180	0.002
Al	0.1402876814×10^{4}	1.000138	0.0309117714	1.9097388902	0.011243	0.002
Si	0.17656111084×10	1.000018	0.0303687190	1.9021837210	0.012135	0.002
P	0.2186313774×10^{4}	1.000000	0.0424440383	1.8803796984	0.010772	0.002
S	0.2669472820×10^{4}	1.000005	0.0489589594	1.8709900401	0.010618	0.002
Cl	0.3219178700×10^{4}	0.999972	0.0589438067	1.8557109540	0.010508	0.002
Ar	0.3839790833×10^{4}	1.000012	0.1328763086	1.8197832987	0.008120	0.001
K	0.4539154495×10^{4}	1.000578	0.0246332858	1.9591189535	0.019954	0.024
Ca	0.5320605746×10^{4}	1.000885	0.0296388407	1.9722121308	0.018028	0.009
Sc	0.6183371002×10^{4}	1.000821	0.0239192856	1.9945777721	0.010397	0.006
Ti	0.7134347345×10^{4}	1.000755	0.0265441851	1.9948515790	0.009924	0.005
V	0.8178132891×10^{4}	1.000701	0.0298180821	1.9924129997	0.009493	0.005
Cr	0.9314933629×10^{4}	1.000637	0.0330506124	1.9503132017	0.009097	0.005
Mn	0.1056137959×10^{5}	1.000609	0.0322891792	1.9606106511	0.009183	0.005
Fe	0.1191012264×10^{5}	1.000588	0.0407474907	1.9608370071	0.016950	0.005
Co	0.1336884777×10^{5}	1.000547	0.0418099810	1.9484575704	0.008086	0.004
Ni	0.1494214268×10^{5}	1.000526	0.0448690512	1.9303267139	0.019237	0.008
Cu	0.1662690689×10^{5}	1.000497	0.0281202960	1.7912255000	0.009202	0.012
Zn	0.1844947108×10^{5}	1.000486	0.0139972708	1.9568985420	0.004872	0.009
Ga	0.2039910960×10^{5}	1.000468	0.0148340246	1.9726902687	0.004484	0.007
Ge	0.2248213834×10^{5}	1.000451	0.0169150404	1.9479095480	0.004802	0.007
As	0.2470302422×10^{5}	1.000428	0.0065178488	2.0448703464	0.004429	0.017
Se	0.2706668768×10^{5}	1.000426	0.1052039355	2.0264542614	0.001166	0.051
Br	0.2957710255×10^{5}	1.000423	0.1194026181	1.9978975985	0.006559	0.002
Kr	0.3223836707×10^{5}	1.000390	0.1384007539	1.9748871400	0.007794	0.006
Rb	0.3506036512×10^{5}	1.000391	0.0243149975	1.9563931873	0.022411	0.030
Sr	0.3804560626×10^{5}	1.000368	0.0423966415	1.8820647718	0.013481	0.020
Y	0.4119170231×10^{5}	1.000308	0.0324988842	1.8008987990	0.041228	0.311
Zr	0.4450829106×10^{5}	1.000443	0.0475553764	1.8236198506	0.013601	0.033
Nb	0.4799179393×10^{5}	1.000460	0.0561513020	1.9602114265	0.011764	0.087
Mo	0.5165771156×10^{5}	1.000453	0.0628798335	1.9025810029	0.010182	0.009
Tc	0.5551228592×10^{5}	1.000437	0.0603410279	1.9317383336	0.013438	0.098
Ru	0.5954034580×10^{5}	1.000423	0.0599624251	1.9285028719	0.013132	0.089
Rh	0.6376629944×10^{5}	1.000413	0.0592981861	1.9829806006	0.010719	0.099
Pd	0.6818119701×10^{5}	1.000398	0.0243923125	2.2848207456	0.004794	0.054
Ag	0.7280973386×10^{5}	1.000404	0.0227734986	2.3111741820	0.004418	0.092
Cd	0.7764811118×10^{5}	1.000395	0.0285738056	2.2883639708	0.004594	0.118
In	0.8269282243×10^{5}	1.000379	0.0537077197	2.0539527671	0.008217	0.016
Sn	0.8795276411×10^{5}	1.000395	0.0326036858	2.1383309733	0.011556	0.009
Sb	0.9343120690×10^{5}	1.000383	0.0257251787	2.2005023947	0.010045	0.017
Te	0.9913364561×10^{5}	1.000370	0.0099282829	2.1999991501	0.011112	0.016
I	0.1050645522×10^{6}	1.000367	0.0099007596	2.1999865037	0.012297	0.019
Xe	0.1112278513×10^{6}	1.000357	0.0287047070	2.2009214000	0.009487	0.020

two parameters characterizing the nonconvexity, namely, the abscissa of the most negative $\rho''(r)$, r_{min}, and the width Δr of the nonconvex region.

In Fig. 5 we see that Koga's densities behave very much as the densities of Clementi and Roetti do [27], in spite of the clear structural differences between these two HFR solutions. The approximate densities copy quite well this pattern with four exceptions: Zn, Ga, and Rh, which are nonconvex in Koga's picture but convex in the approximate representation, and the As atom, that behaves in the opposite way. We notice that the nonconvex width is smaller than 0.25 bohr for all but three atoms (Li, Be, and B). This means that Δr is a quite demanding test for an approximate density.

We use the $B(r)$ function in Eq. (39) to further examine the fitness of the $F(r)$ functions. Starting from the general inequality for $\rho(r)^{1/2}$ established by the Hoffmann-Ostenhof's expression [25]

$$-\frac{1}{2}\nabla^2\sqrt{\rho(r)} + [\epsilon - V(r)]\sqrt{\rho(r)} \leq 0 \ , \qquad (40)$$

Table 2. Details of the approximate density, $F(r)$, and its first and second derivatives for the Fe atom

$p = DIM(\mathbf{f}(\mathbf{r})) = 20$
$\alpha = 0.0407474907$
$\beta = 1.9608370071$
$\Delta_{\text{opt}} = 0.6048495038 \times 10^{-12}$
$A = 1.0005884569$
$\delta_{\max}/\rho(r_{\max}) = 5.0921062939 \times 10^{-5}$
$r_{\max} = 0.0169498462$
$-F''(0)/(2F'(0)) = 26.176622694$

i	$C_i/F(0)$	ζ_i
1	$0.9649518942 \times 10^{-9}$	$4.0747490749 \times 10^{-2}$
2	$0.1571926122 \times 10^{-6}$	$7.9899187808 \times 10^{-2}$
3	$0.1431049569 \times 10^{-5}$	$1.5666928429 \times 10^{-1}$
4	$0.2107663992 \times 10^{-5}$	$3.0720293052 \times 10^{-1}$
5	$0.6076501237 \times 10^{-5}$	$6.0237487485 \times 10^{-1}$
6	$0.7306313448 \times 10^{-4}$	1.1811589468
7	$0.4578723738 \times 10^{-3}$	2.3160601741
8	$0.4981020591 \times 10^{-3}$	4.5414165001
9	$-0.1651900160 \times 10^{-2}$	8.9049775381
10	$0.4501248107 \times 10^{-2}$	$1.7461209504 \times 10^{1}$
11	$0.1471842873 \times 10^{-2}$	$3.4238585785 \times 10^{1}$
12	$0.9992197236 \times 10^{-1}$	$6.7136286079 \times 10^{1}$
13	$-0.1069256635 \times 10^{-1}$	$1.3164331426 \times 10^{2}$
14	$-0.6034992170 \times 10^{-2}$	$2.5813108235 \times 10^{2}$
15	$-0.1404465336 \times 10^{-2}$	$5.0615297895 \times 10^{2}$
16	$-0.1382653724 \times 10^{-2}$	$9.9248349239 \times 10^{2}$
17	$0.1701684332 \times 10^{-3}$	$1.9460983608 \times 10^{3}$
18	$-0.1240901515 \times 10^{-2}$	$3.8159816854 \times 10^{3}$
19	$0.8504584231 \times 10^{-3}$	$7.4825181072 \times 10^{3}$
20	$-0.4593120463 \times 10^{-3}$	$1.4671998411 \times 10^{4}$

$F(0) = +0.1191012264 \times 10^{5}$
$F'(0) = 0.6196908240 \times 10^{6}$
$F''(0) = +0.3244282577 \times 10^{8}$

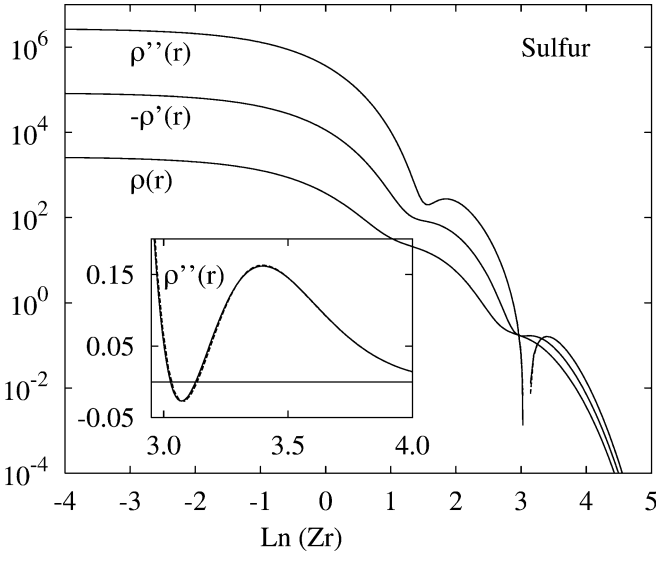

Fig. 2. Logarithmic plots of $\rho(r)$, $\rho'(r)$, and $\rho''(r)$ for the S atom. *Solid lines* and *dotted lines* (hidden behind the solid lines) stand for reference and approximate functions, respectively. The inset shows the small nonconvex region near $r \sim 1.39$ bohr

and taking for $V(r)$ the bare Coulomb potential, the following inequality can be readily found for $B(r)$ [26]

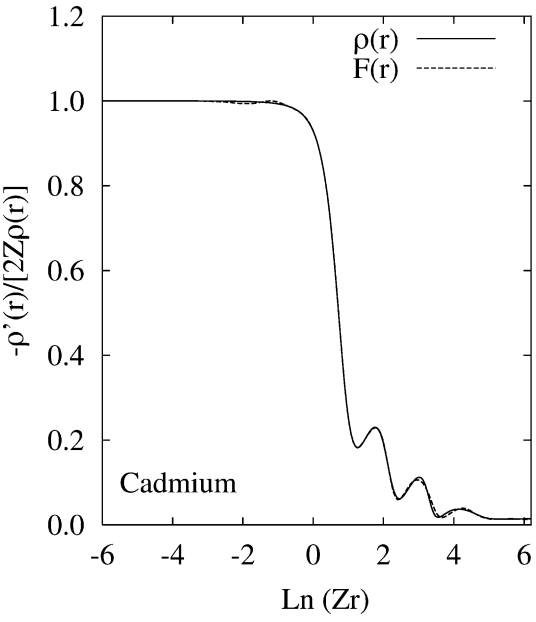

Fig. 3. $\rho'(r)/[2Z\rho(r)]$ for Cd. *Solid (dotted) lines* stand for the reference (approximate) density

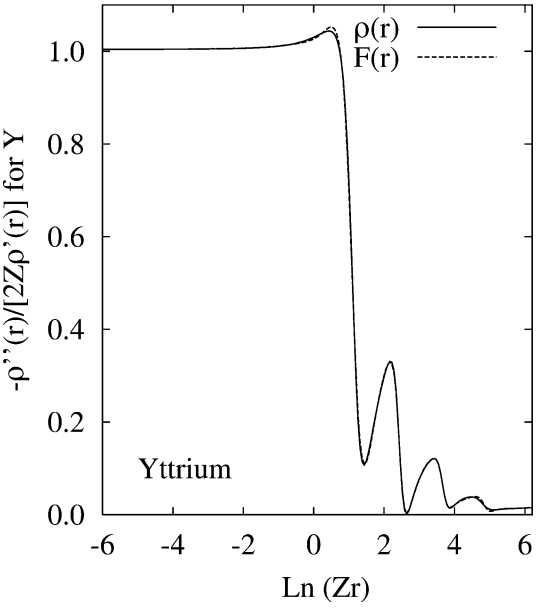

Fig. 4. $\rho''(r)/[2Z\rho'(r)]$ for Y. *Solid (dotted) lines* stand for the reference (approximate) density

$$B(r) \geq \frac{1}{Zr}\left(\frac{A(r)-1}{A(r)}\right) + \frac{1}{2}A(r) + \frac{\epsilon}{Z^2 A(r)} = C(r) \ , \tag{41}$$

say, where $A(r)$ is the function in Eq. (39). Equation (41) sets a lower limit to $B(r)$ for any r, including $r = 0$. If the density exactly fulfils the cusp condition, the $r = 0$ limit of the $C(r)$ function is finite, namely

$$\lim_{r\to 0} C(r) = C(0) = -2B(0) + \frac{5}{2} + \frac{\epsilon}{Z^2} \ , \tag{42}$$

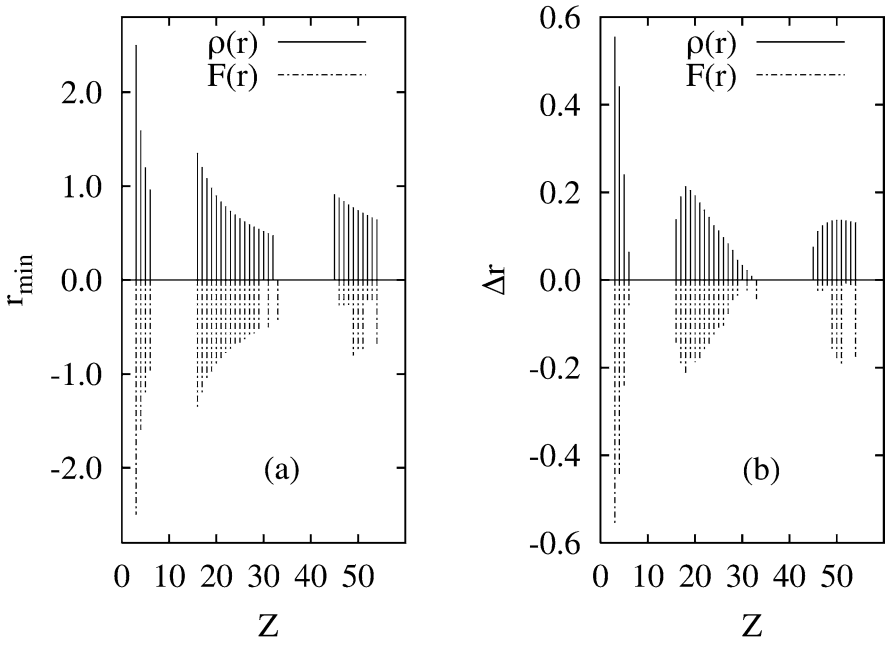

Fig. 5. a Values of r at the minimum of the nonconvexity region and **b** the width of this region. *Solid lines* stand for the reference density. *Dotted lines* stand for (the negative of) the approximate density

and we find the well-known lower limit for $B(r)$ at the origin [27], $B(0) \geq \frac{5}{6} + \frac{c}{3Z^2} = B_L$. If the density does not fulfil the cusp condition exactly, as is the case for the reference densities used in this work, $A(0) \neq 1$. Then $\lim_{r\to 0} C(r) = +\infty$ if $A(0) > 1$ and $\lim_{r\to 0} C(r) = -\infty$ if $A(0) < 1$. Thus, densities with $A(0) > 1$ do not obey the BCF inequality in Eq. (41) in regions very close to the nucleus.

We also examined the radial function

$$K(r) = B(r) - C(r) \ , \tag{43}$$

which must be nonnegative according to Eq. (41). To avoid the wrong behaviour at very small distances, we corrected $A(r)$ with a uniform shift, $A(r) \to A'(r) = A(r) - [A(0) - 1]$, that is about 10^{-4} for all cases in this study. It is unobservable in Fig. 6, where we plot $K(r)$ for the rare-gas atoms for $0 \leq r \leq 20$ bohr. We see that $K(r)$ is nonnegative in this range and that the inequality in Eq. (41) is fulfilled for all distances of practical interest in these four cases. $K(r)$ has a clear shell structure that is essentially the same for all atoms in a period, with a number of maxima equal to $n - 1$, suggesting that it is an effect of the bare Coulomb potential. The matching of this structure by the approximate density is qualitatively correct for the four atoms. The quantitative performance is excellent for Ne and Ar, and very good for Kr. The deviations for $u > 0.92$ are physically meaningless because the density there is much smaller than the numerical precision of the calculation.

3.3 Density functionals

We briefly present here selected results that illustrate the performance of the approximate densities in the calculation of specific density integrals. We will refer to functionals involving fractional powers of $\rho(r)$ and examine relative deviations of the form

$$\Delta_s = 100 \times \frac{\int_0^\infty [\rho^{s/3}(r) - F^{s/3}(r)] r^2 \mathrm{d}r}{\int_0^\infty \rho^{s/3}(r) r^2 \mathrm{d}r} \ . \tag{44}$$

The Z dependence of this deviation for three functionals is shown in Fig.7: the Thomas–Fermi kinetic energy, Δ_k ($s = 5$), the Thomas–Fermi exchange energy, Δ_x ($s = 4$), and the Wigner correlation energy, Δ_c [39], all calculated with the numerical integration scheme of Pérez–Jordá and coworkers [29]. The performance of the approximate densities is uniformly good, with the exceptions of Mo and In. All other atoms but Tc give relative deviations smaller than 0.05% for the three integrals. The two peaks in Fig. 7 are very annoying, particularly if one realizes that the atomic configurations of Mo and In atoms do not differ in an essential way from those of their neighbours in the periodic table. To explore this issue in depth we computed Δ_k, Δ_x, and Δ_c for Tc, Mo, and In using the $F(r)$ functions obtained by fitting the Clementi and Roetti densities [15]. For the three atoms and the three functionals the relative deviation is always smaller than 0.002%. This fact shows once again that the density used as a reference affects more the performance of the fitting procedure than the specific configuration or electronic state of the atom considered.

The density functional associated with the two-thirds power of the electron density is particularly interesting owing to its detailed shell structure. The plot of this integral in Fig. 8 shows that the performance of the approximate densities is excellent with the single exception of the As atom, where we find insufficient accuracy in the numerical integration. An 80-point Laguerre quadrature [40] reduces the deviation for this case to a quarter of the value depicted in the figure. This shell structure correlates with the electron occupation of the atomic orbitals and it can be described in terms of the

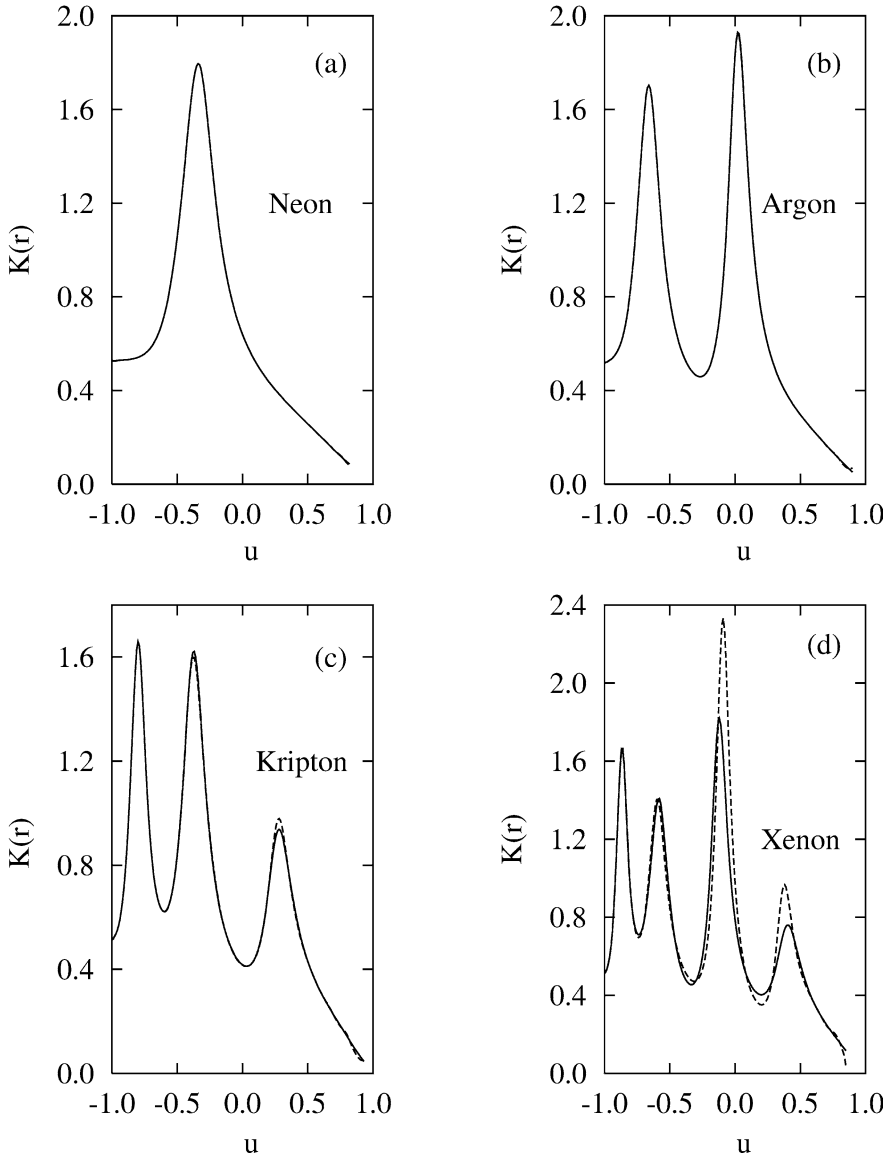

Fig. 6. Test function $K(r)$, Eq. (43), for Ne, Ar, Kr, and Xe. *Solid lines* and *dotted lines* stand for the reference and the approximate densities, respectively. $u = (r - \langle r \rangle)/(r + \langle r \rangle)$

electron configurations selected in the reference calculation [21]. The functional increases from the $(ns)^1$ to the $(ns)^2$ states but it uniformly decreases while filling the *np* orbitals, up to the 5*p* states, where the effect vanishes. The filling of the 3*d* block shows that the $(4s)(3d)^{x+1}$ configuration, a more internal distribution than the $(4s)^2(3d)^x$ one, gives a smaller value for this integral. Within the 4*d* block, Y, Zr, Tc, and Cd have $(5s)^2(4d)^x$ ground configurations and this functional is linear in Z, whereas Nb, Mo, Ru, Rh, and Ag, having $(5s)^1(4d)^{x+1}$ configurations, lie on a nearly parallel line of smaller intercept. The last member of this block, the Pd atom, has a $(5s)^0(4d)^{10}$ configuration and shows a drop in this quantity comparable to those of the rare-gas atoms. All these electronic features, due to the action of the electron repulsion, are quantitatively reproduced by the approximated densities.

Finally, we present two quality measures related to the Shannon entropy. The first one shows the integrand of the N-normalized entropy as a function of the radial coordinate. This function is a demanding test for any approximate density owing to its shell structure. The case of the iodine atom is plotted in Fig. 9. The integrand goes to zero at small and large distances, being negligible for $5 \times 10^{-4} \geq r \geq 3.0$ bohr. Its shell structure, as that of the $K(r)$ function (Eq. 43), is entirely determined by the principal quantum number, with $n - 1$ maxima. The approximate density follows the reference pattern extremely well.

The second entropy measure is the Z dependence of the unit-normalized entropy $S_1 = -\langle \ln \rho \rangle_1 = -4\pi \int_0^\infty \bar{\rho}(r) \ln \bar{\rho}(r) r^2 \mathrm{d}r$, with $\bar{\rho}(r) = \rho(r)/N$. This quantity shows the structure of the N-normalized expectation value of the minus-one-third power of $\rho(r)$, namely $\langle \rho^{-1/3} \rangle_N = 4\pi N^{-1} \int_0^\infty \rho^{2/3} r^2 \mathrm{d}r$, as we see in Fig. 10. Again, the approximate densities reproduce quantitatively the results of the reference functions for all atoms. This completes our appraisal of the $F(r)$ densities.

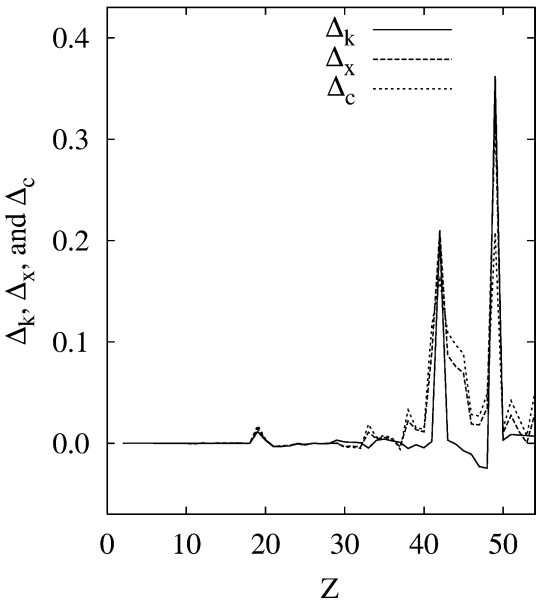

Fig. 7. Relative deviations (percent) of the Thomas–Fermi kinetic energy, Δ_K, the exchange energy, Δ_X, and the Wigner correlation energy, Δ_c, for He–Xe

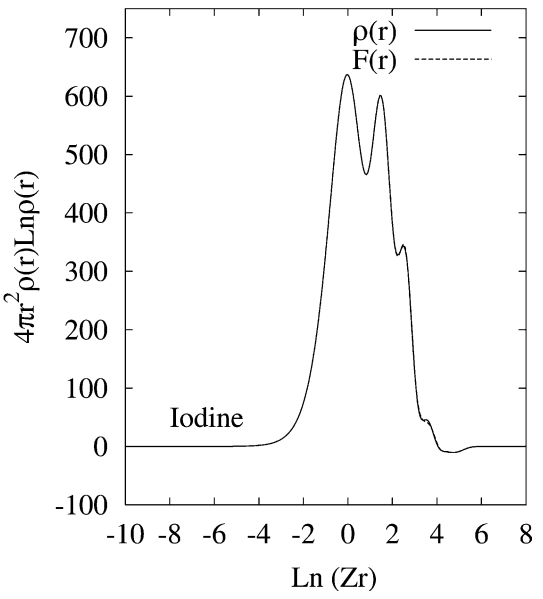

Fig. 9. Integrand of the Shannon entropy for the iodine atom. *Solid (dotted) lines* stand for reference (approximate) densities, respectively

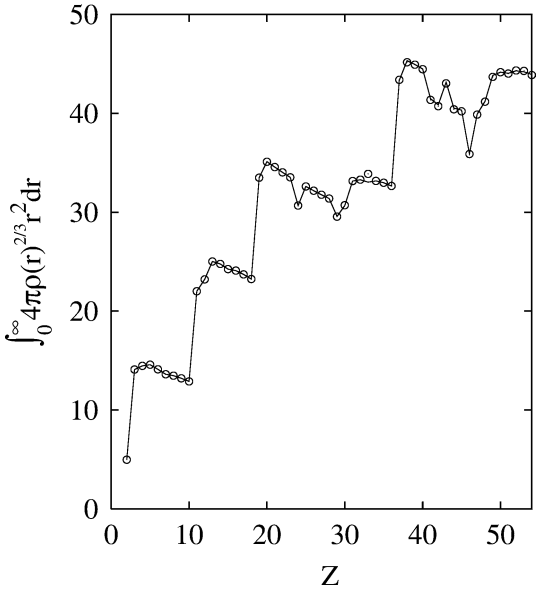

Fig. 8. Z dependence of the $\langle\rho^{-1/3}\rangle$ functional for atoms He–Xe. The *solid line* stands for the reference densities and the symbols stand for approximate densities

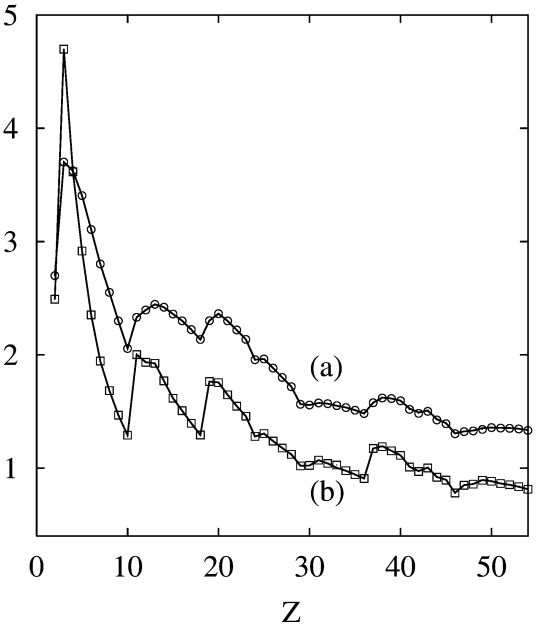

Fig. 10. a Unit-normalized Shannon entropy $-\int_0^\infty 4\pi r^2[(\rho(r)/N)]$ $\ln[(\rho(r)/N)]dr$, and **b** $\langle\rho^{-1/3}\rangle$ functional $N^{-1}\int_0^\infty 4\pi r^2\rho^{2/3}dr$, for atoms He–Xe. *Solid lines (symbols)* stand for reference densities (approximate) densities

4 Concluding remarks

We have presented a method to fit a linear combination, $F(r)$, of 1s–type Gaussian functions plus a 1s–type exponential function to a high–quality radial atomic density, $\rho(r)$. The fitted density and its first and second derivatives are forced to equal the corresponding reference values at the origin. Additional restrictions are imposed on $F(r)$ in order to have exact matching of the $\langle r^k\rangle$ moments ($k = -2, \ldots, +6$) of $\rho(r)$. Using the high-quality nonrelativistic HFR densities of Koga et al. [21] as a reference, we obtained accurate analytical representations for atoms He–Xe. The presence of a single exponential component gives the required flexibility to obtain quantitative results with basis sizes comparable to those used in the all-exponential approximations. The performance of the proposed algorithm was evaluated by measuring the response of $F(r)$, $F'(r)$

and $F''(r)$ to a series of demanding tests, including the shell structure of $\rho''(r)$, the location and shape of the nonconvexity regions of the density, and the Z dependence of several functionals which are important in density functional theory. With a few exceptions, the structural features of these selected properties are quantitatively reproduced by the approximate densities. These results make of them uniformly adequate research tools for atomic, molecular, and solid–state calculations.

Acknowledgements. The authors thank Domingo González for his inspiring suggestions. Fruitful discussions with V. Luaña, J. M. Recio, and M. Bermejo are gratefully acknowledged. This work was supported by the Spanish Dirección General de Investigación Científica y Técnica, projects nos BQU2000-0466 and BQU2003-06553.

References

1. Bader RFW (1990) Atoms and molecules.Oxford University Press, Oxford
2. Becke AD, Edgecombe KE (1990) J Chem Phys 92: 5397
3. Silvi B, Savin A (1994) Nature 371: 683
4. Savin A, Nesper R, Wengert S, Fäsler TF (1997) Angew Chem Int Ed Engl 36: 1808
5. Meyer B, Hummler K, Elsäser C, Fähnle M (1995) J Phys Condens Matter 7: 9201
6. Vyboishchikov SF, Sierraalta A, Frenking G (1996) J Comput Chem 18: 416
7. Cioslowski J,Piskorz P (1996) Chem Phys Lett 255: 315
8. Trail JR, Bird DM (1999) Phys Rev B 60: 7863
9. Koritsanszky TS, Coppens P (2001) Chem Rev 101: 1583
10. Hirshfeld FL (1977) Theor Chim Acta 44: 129
11. Spackman MA, Byrom PG (1997) Chem Phys Lett 267: 215
12. McKinnon JJ, Mitchell AS, Spackman MA (1998) Chem Eur J 4: 2136
13. McKinnon JJ, Mitchell AS, Spackman MA (1998) Chem Commun 19: 2071
14. Martín Pendás A, Costales A, Luaña V (1998) J Phys Chem B 102: 6937
15. Clementi E and Roetti C 1974 At Data Nucl Data Tables 14: 177
16. McLean AD, McLean RS (1981) At Data Nucl Data Tables 26: 197
17. Bunge CF, Barrientos JA, Bunge AV, Cogordan JA (1992) Phys Rev A 46: 3691
18. Koga T, Tatewaki H, Thakkar AJ (1993) Phys Rev A 47: 4510
19. Koga T, Thakkar AJ (1993) Phys Rev A 48: 4775
20. Koga T, Thakkar AJ (1994) Phys Rev A 50: 891
21. Koga T, Watanabe S, Kanayama K, Yasuda R, Thakkar AJ (1995) J Chem Phys 103: 3000
22. Koga T (1997) Theor Chim Acta 95: 113
23. Cioslowski J, Piskorz P, Rez P (1997) J Chem Phys 106: 3607
24. (a) Kato T (1957) Commun Pure Appl Math 10: 151; (b) Steiner EJ (1963) J Chem P hys 39: 2365; (c) Yue CP, Chong DP (1968) Theor Chim Acta 12: 431; (d) Chapm an JA, Chong DP (1979) Can J Chem 48: 2722
25. Hoffmann-Ostenhof M and Hoffmann-Ostenhof T (1977) Phys Rev A 16: 1782
26. Esquivel RO, Chen J, Stott MJ, Sagar RP, Smith VM Jr (1993) Phys Rev A 47: 936
27. Esquivel RO, Sagar RP, Smith VA Jr, Chen J and Stott MJ (1993) Phys Rev A 47: 4735
28. Martín Pendás A, Álvarez Blanco M, Costales A, Mori Sánchez P, Luaña V (1999) Phys Rev Lett 83: 1930
29. (a) Pérez–Jordá JM, San–Fabián E, Moscardó F (1992) Comput Phys Commun 70: 271; (b) Pérez–Jordá JM, San–Fabián E (1993) Comput Phys Commun 77: 46; (c) Pérez–Jordá JM, Becke A, San–Fabián E (1994) J Chem Phys 100: 6520
30. Powell MJD (1965) Comput J 7: 303
31. Gálvez FJ, Porras I (1991) Phys Rev A 44: 144
32. Porras I, Gálvez FJ (1992) Phys Rev A 46: 105
33. Angulo JC, Dehesa JS, Galvez FJ (1990) Phys Rev A 42: 641
34. Angulo JC, Dehesa JS (1991) Phys Rev A 44: 1516
35. Antolín J, Zarzo A, Angulo JC (1993) Phys Rev A 48: 4149
36. Angulo JC, Schmider H, Sagar RP and Smith VH Jr (1994) Phys Rev A 49: 726
37. Angulo JC, Yanez RJ, Dehesa JS,Romera R (1996) Int J Quantum Chem 58: 11
38. Angulo JC, Romera R , Dehesa JS (2000) J Math Phys 41: 7906
39. Clementi E, (1990) Modern techniques in computational chemistry, MOTECC-90, ESCOM Leyden
40. Francisco E, Recio JM, Álvarez Blanco M, Martín Pendás A, Pueyo L (1995) Phys Rev B 51: 2703